 

*INTERACTION OF LASER RADIATION WITH MATTER. LASER PLASMA*

PACS numbers: 42.60.By; 52.57.–z; 52.38.Ph
DOI: 10.1070/QE2014v044n03ABEH015314

# Numerical analysis of radiation dynamics in a combined hohlraum in the X-ray opacity experiments on the 'Iskra-5' laser facility

S.V. Bondarenko, G.V. Dolgoleva, E.A. Novikova

*Abstract.* **We report the results of numerical analysis of radiation dynamics (laser absorption and X-ray generation) by using SND-LIRA code in a combined box used in the X-ray opacity measurements on the 'Iskra-5' facility (laser radiation wavelength, $\lambda$ = 0.66 μm; laser pulse duration, $\tau_{0.5} \approx 0.6$ ns; and energy, 900 J). Combined boxes used in these experiments comprised three sections: two illuminators delivering laser radiation and a central diagnostic section with a test sample. We have proposed a scheme for step-by-step calculation of the heating dynamics of the sample under study in a three-section hohlraum. Two designs of a combined box, which differ in the ways the laser radiation is injected, are discussed. It is shown that the axial injection of the beams results in intense secondary laser irradiation of the illuminator edge which leads to its partial disruption and penetration of laser radiation into the central diagnostic section. In this case the sample under study is exposed to additional uncontrolled action of scattered laser radiation. Such an undesirable action may be avoided by using the lateral injection of the beams through four holes on the lateral side of the illuminators. For the latter case we have calculated the heating dynamics for the sample and found an optimal time delay for an X-ray probe pulse.**

***Keywords:*** *opacity, X-ray combined holhraum, numerical analysis by SND-LIRA software.*

## 1. Introduction

High-power pulsed laser facilities suggest unique possibilities for attaining a high energy density in small volumes of a substance. Measurements of X-ray opacity in a substance heated to a high temperature (from 50 to 100 eV and more) is an attractive field of investigations. In such experiments the material of the sample under study is heated by X-ray radiation generated inside a holhraum. In the experiments on the 'Iskra-5' laser facility we employed a three-section hoalhraum comprised of a central part (diagnostic section) where the sample was placed, and two lateral sections (illuminators) in which the injected laser radiation was absorbed. To prevent the sample from undesirable laser heating the diagnostic section was separated from lateral sections by a film with a deposited layer of material having a large atomic number. The thicknesses of the film and coatings were chosen to provide an efficient transmission of X-ray radiation into the diagnostic section.

The experiments on studying X-ray opacity in heated aluminium and germanium samples of thickness ~0.1 μm enclosed between two plastic layers of thickness ~1 μm have been performed on the Iskra-5 facility. The experiments as well as the methods of measurements and results obtained were described in [1]. Results of the numerical-theoretical analysis of a fine structure of X-ray absorption spectra for aluminium and germanium based on the improved Slater average-ion model are presented in [2]. The aim of the present work is a numerical simulation of the dynamics of radiation fields in a holhraum of complex geometry and finally determination of the regime of heating and gas-dynamic expansion of the sample under investigation.

For analysing the results of opacity measurements one should know the sample conditions (the density and temperature distributions over the sample volume) at the instant of hard X-ray backlightning. The dynamics of the field of X-ray radiation and its spectral characteristics are determined by the lasing conditions on internal surfaces of the side sections (illuminators) of the holhraum. It is important to know the positions and dimensions of laser radiation spots, the intensity of the light field and the fraction of absorbed laser energy. The X-ray radiation passed through the material of a film–converter, on the one hand, directly affects the sample material and, on the other hand, heats the material of walls of the diagnostic section. Thus, the sample is subjected to an action of both the linear X-ray radiation from the domains of primary and secondary laser spots, partially attenuated in passing through the film converter material, and the quasi-equilibrium radiation of holhraum walls.

The dynamics of radiation fields of a combined X-ray holhraum was analysed by using the numerical SND-LIRA code [3, 4]. The calculations were performed in two stages. At the first stage, the conditions were modelled for absorption of laser radiation in the side sections (illuminators) and the parameters were determined for the X-ray radiation from domains of primary and secondary laser spots as well as from domains residing beyond the zones with high laser brightness. Fluxes of laser and X-ray radiation passing to various parts of the partition between the sections (film converter) were calculated. These fluxes were then used as boundary conditions for calculating specific irradiation of the film converter and characteristics of the X-ray radiation passed through it. At the

**S.V. Bondarenko, E.A. Novikova** Russian Federal Nuclear Centre 'All-Russian Research Institute of Experimental Physics', prosp. Mira 37, 607190 Sarov, Nizhnii Novgorod region, Russia;
e-mail: sergvicbond@inbox.ru, novikova@md08.vniief.ru;
**G.V. Dolgoleva** M.V. Keldysh Institute for Applied Mathematics, Russian Academy of Sciences, Miusskaya pl. 4, 125047 Moscow, Russia; e-mail: dolgg@list.ru

Received 19 September 2013; revision received 17 December 2013
*Kvantovaya Elektronika* **44** (3) 217–224 (2014)
Translated by N.A. Raspopov

second stage, the characteristics of X-ray radiation in the diagnostic section were calculated and the heating regime was determined for the sample under study. In this case, we neglected the reciprocal influence of quasi-thermal radiation from the central section of the holhraum on the state of the material and characteristics of radiation from its lateral sections. It was explained, first, by a lower density of the radiation energy in the diagnostic section and, second, by a time delay of generated X-ray radiation in the central section.

Two variants of a combined holhraum design were considered differing in the positions of laser radiation entrance holes. In the first variant, two laser beams passed into each of two edge holes of the illuminators. In the second variant, the laser beams passed through four holes on lateral surfaces of the illuminators.

## 2. Axial injection of laser radiation

The scheme of the experiments on investigating X-ray opacity on the 'Iskra-5' laser facility [1] is shown in Fig. 1. In these experiments the sample under study was placed in the central section of a three-section holhraum. Second-harmonic radiation ($\lambda = 0.53$ μm) of a neodymium laser was injected through axial holes to inner volumes of two lateral sections-illuminators (two beams to each section) separated from the central section by a plastic film with a deposited gold layer of thickness 0.1 μm. The internal surface of the holhraum was deposited by the gold layer of thickness ~1 μm for more efficient energy conversion of the laser driver to X-ray radiation. The heated sample was examined by hard X-ray backlight radiation. The comparison of spectra of the X-ray radiation passed through the sample material with the spectrum of the radiation source makes it possible to determine absorption spectral characteristics of the material.

Calculation by the SND-LIRA code simulated the process of heating of the combined holhraum of diameter 1.0 mm by four laser beams with the total energy $E_L \approx 900$ J and pulse duration $\tau_{0.5} = 0.675$ ns injected into the internal space of lateral sections-illuminators through the axial holes with a diameter of 600 μm. The length of each section was 1.2 mm.

The laser beams injected through the lateral holes fall to a cylindrical surface of the illuminators at a large angle (~60° with respect to the normal). Under these conditions, only a part of laser radiation is absorbed in the spots of primary illumination. The laser beams reflecting from the cylindrical surface of the illuminator are focused in the direction perpendicular to its axis, which results in the formation of zones of intense secondary irradiation. The transverse dimensions of the laser beams were $30 \times 30$ cm; they were focused by the lens objective with a focal length $F = 1600$ mm.

In order to reveal the character of energy redistribution of reflected laser radiation on the internal illuminator surfaces we performed calculations with the model absorption coefficient

$$k = k_0 \cos^3\theta, \tag{1}$$

where $k_0 = 0.5$, and $\theta$ is the angle of radiation incidence onto the surface.

Let us define applicability of formula (1) more exactly. In the considered conditions, the absorption of laser radiation mainly occurs through the inverse bremsstrahlung mechanism. Aspects of propagation and absorption of optical radiation in plasma were thoroughly described in monograph [5]. It is known that transverse electromagnetic waves cannot propagate in plasma with a density $\rho$ exceeding the critical density

$$\rho_c = 1.87 \times 10^{-3} \frac{A}{Z\lambda^2}, \tag{2}$$

where $A$ and $Z$ are the atomic weight and degree of ionisation of the plasma material, respectively; and the density is measured in g cm$^{-3}$ and the wavelength – in microns. Near the critical surface on which at a prescribed wavelength the real part of plasma dielectric function

$$\varepsilon(\omega) = 1 - \frac{\omega^2}{\omega_p^2} = 1 - \frac{\rho}{\rho_c}$$

turns to zero, the laser radiation is reflected. Here

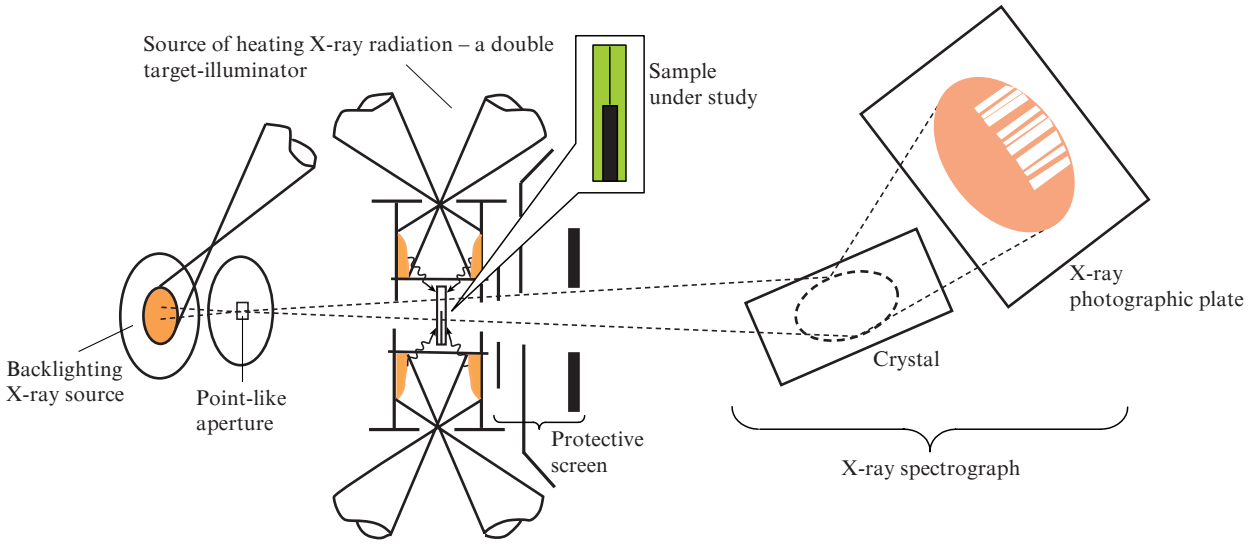


**Figure 1.** Scheme of the experiments on investigating X-ray opacity on the 'Iskra-5' laser facility with the axial injection of laser beams.

$$\omega_p = \left(\frac{4\pi e^2 n_e}{m_e}\right)^{1/2}$$

is the Langmuir frequency; $e$ and $m_e$ are the electron charge and mass, respectively; and $n_e$ is the concentration of the electron gas. Figure 2 shows a characteristic trajectory of the light beam. The light beam falling from vacuum with the refractive index $n = 1$ at an angle $\theta$ reaches the layer of plasma with the refractive index $n = \sin\theta$ ($\rho = \rho_c \cos^2\theta$). Due to a variation of the refractive index in this layer, the trajectory of the light beam bends (light refraction).

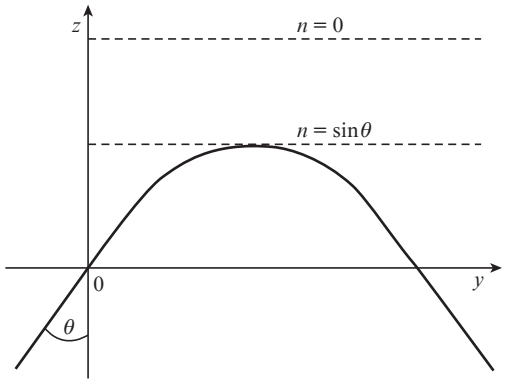


**Figure 2.** Typical trajectory of a light beam in plasma.

The imaginary part of the plasma dielectric function responsible for the absorption of electromagnetic waves is caused by collisions of charged particles. We will assume that plasma heated by laser radiation is isothermal and uniform in the charge composition. In this case, the absorption of laser energy per unit length is proportional to the square of the plasma density:

$$k_{st} = a\rho^2\lambda^2 \ln\Lambda_{ei} \propto \rho^2 \qquad (3)$$

(the Coulomb logarithm $\ln\Lambda_{ei}$ weakly depends on plasma parameters; hence, we will consider it constant). The absorption coefficient

$$k = 1 - e^{-\tau} \qquad (4)$$

is determined by the total optical thickness $\tau = \int k_{st}(s)ds$ along the trajectory of light propagation, in which the coordinate $s$ is counted. First of all, most interesting is the situation where at large angles of incidence $\theta$, the absorption of laser radiation substantially falls in near-wall plasma. Because a considerable part of laser energy in this case is reflected, the optical thickness $\tau$ is not large and in (4) we may retain only the first term of expansion in series $k \approx \tau$. The flow of near-wall plasma can be approximately described by using the isothermal rarefaction model which is characterised by an extremely severe (exponential) density distribution. This means that the entire optical thickness $\tau$ in (4) is 'acquired' in the range of maximal densities along the beam trajectory, i.e., near the turning point where $\rho \approx \rho_c \cos^2\theta$. The distance $\Delta s$ covered by the beam in the medium at an angle of incidence $\theta$ is inversely proportional to the cosine of this angle: $\Delta s \propto 1/\cos\theta$. Hence, $\tau \approx k_{st}\Delta s \propto \cos^3\theta$ and we arrive at the angular dependence (1).

The scheme of laser illumination of the inner surface of the illuminator is shown in Fig. 3. One can see that reflected laser radiation forms the spots of intense secondary irradiation on the surface of the film screen, in which the brightness is higher than in the primary spots. This is the result of the laser beam reflection from the inner surface of a cylindrical mirror in the case where the axis of the light beam crosses that of the reflecting cylindrical surface.

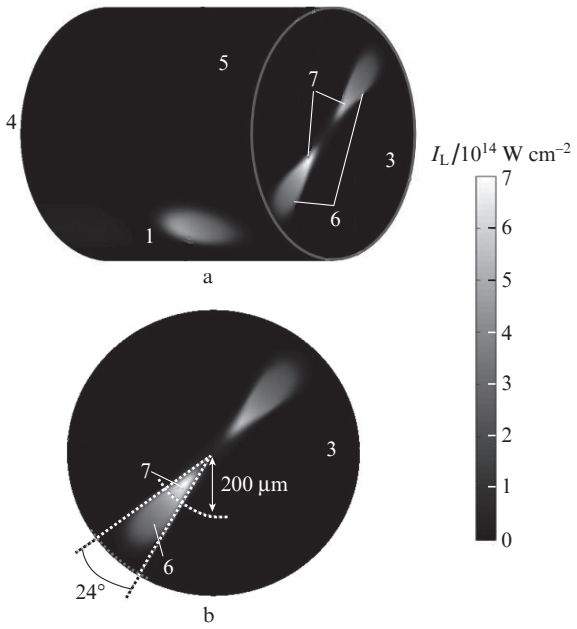


**Figure 3.** Schematic sector partitioning of the internal surface of the illuminators: (a) general view and (b) sector positions in the domain of secondary laser spots on the film converter:
(1, 2) spots of primary irradiation; (3) film–converter; (4) axial surface of the illuminator; (5) lateral surface of the illuminator outside laser spots; (6, 7) zones of secondary laser spots; sector 2 resides at the opposite (with respect to the axis of symmetry) side of the cylindrical surface of the illuminator.

To perform the numerical simulation adequate to the experimental conditions one should take into account an influence of zones of intense secondary irradiation. The scheme of sector partitioning of the inner illuminator surface, used in the calculations by the SND-LIRA code is also presented in Fig. 3 (see also Table 1).

Figure 4 shows the time dependence of the laser absorption coefficient in primary spots obtained from the calculations by the SND-LIRA code (a maximal intensity of the laser pulse corresponds to the instant $t = 1.0$ ns). One can see that at most 10% of the energy of incident laser radiation is absorbed in the primary spots. The absorption in the secondary spots is much higher because the angles of radiation incidence to a surface are 25°–35°.

Data on the balance of laser energy obtained from calculations by the SND-LIRA code are given in Table 1. One can see that laser radiation is redistributed inside the illuminator and is concentrated in zones of intense secondary laser irradiation on the surface of the film converter. Already in the first half of the laser pulse, the film–converter warms up in these zones (that is, the layers of gold and plastic get rarefied to densities below the critical value) and the laser radiation partially passes to the diagnostic section.

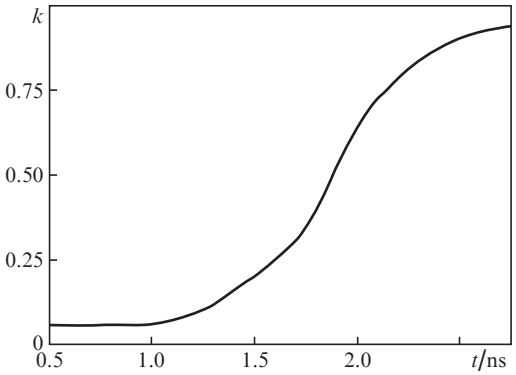


**Figure 4.** Time dependence of the absorption coefficient for laser radiation in laser spots (on surfaces of sectors 1 and 2).

**Table 1.** Balance of laser energy in the illuminator in the case of the axial injection of laser beams.

| Sector number | Sector | $S$/mm$^2$ | $E_L$/J |
|---|---|---|---|
| 0 | Holes | 0.283 | 20.7 |
| 1 | Primary laser spots on the cylindrical surface of | 0.059 | 21.7 |
| 2 | the illuminator | 0.059 | 21.6 |
| 3 | Film converter without secondary spots | 0.695 | 12.1 |
| 4 | Illuminator edge | 0.503 | 43.4 |
| 5 | Cylindrical surface of the illuminator | 3.65 | 13.7 |
| 6 | Secondary laser spots | 0.074 | 208.7 |
| 7 | on the film converter | 0.0167 | 144.3 |
| | $\Sigma$ | 5.34 | 486.2 |

Notes: $S$ is the surface area of a particular sector; $E_L$ is the energy of absorbed (or transmitted by the film converter in sectors 6 and 7) laser radiation.

The energy fluxes of laser radiation (incident, absorbed, reflected and transmitted through the film converter) in the sectors of the film screen are shown in Fig. 5. The material of the film–converter in sector 6 burns through (that is, transmits the laser radiation to the central section) at the instant $t$ = 1.125 ns. The energy of radiation transmitted through the film converter to the diagnostic section of the holhraum is ~20% of the energy of incident laser radiation. In sector 7 (where the laser intensity is three times higher) the burning through occurs at the instant $t \approx 0.95$ ns and the transmittance is 44%. Thus, the laser radiation with the energy of ~200 J passes to the internal volume of the diagnostic section from the side of both lateral sections.

Note that description of the interaction of an inclined incident laser beam (after it reflects from the cylindrical mirror) with the material of the film converter is a difficult problem, which can be analysed in the frameworks of the sector approximation employed in the calculations in general terms only. In particular, it is impossible to predict the direction of propagation for the laser beam after its passage through the material of the film converter. It is not improbable that the sample itself is subjected to substantial action.

Figure 6 shows the time dependences of the effective temperature of irradiation of various areas on the internal illuminator surface. The first spike of X-ray radiation is related to the heating of the film-converter material in the zones of secondary spots. In sector 7, the maximal radiation temperature $T_X$ = 175 eV is attained at $t$ = 0.7 ns, and in sector 6 the maximal temperature $T_X$ = 167 eV is attained at $t$ = 0.85 ns. In following instants, a highly heated (to the electron temperature $T_e$ = 4–5 keV) material of the film–converter in these zones undergoes intensive rarefaction which leads to an abrupt fall of

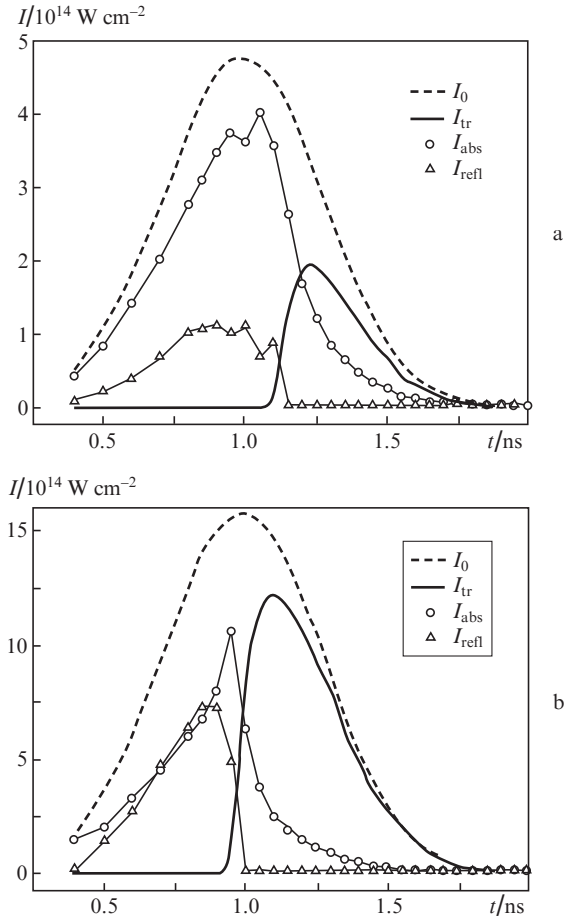


**Figure 5.** Intensities $I_0$, $I_{abs}$, $I_{tr}$ and $I_{refl}$, respectively, for incident, absorbed, passed (through a film converter) and reflected radiation in the secondary laser spot on the film converter in sectors (a) 6 and (b) 7.

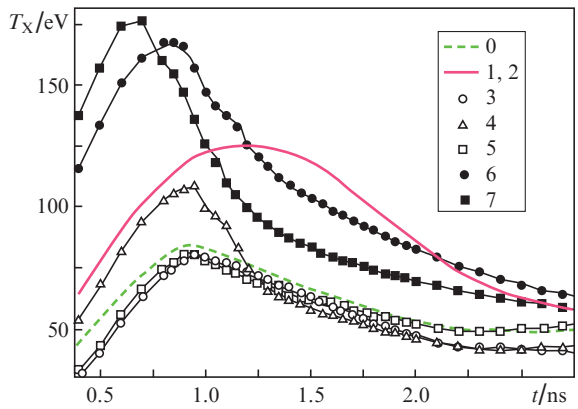


**Figure 6.** Time dependence of the effective temperature of radiation from various domains (sectors) of the internal surface of the illuminator in the case of the axial injection of laser beams. Sector numbers correspond to data presented in Table 1 and Fig. 3.

its X-ray luminosity before the laser pulse ever reaches a maximum. The rise of temperature of the rear edge of the illuminator (sector 4) to 108 eV is related to the heating of its surface by the radiation passing from the zones of secondary laser spots. In the primary laser spots at $t = 1.0–1.5$ ns the radiation temperatures $T_X = 120–130$ eV are attained. The radiation temperature for a lateral surface of the illuminator is not higher than 80 eV. This corresponds to an average effective temperature of the heating radiation falling onto this surface.

X-ray radiation inside the central (diagnostic) section of the holhraum is generated as the result of heating external (coated with gold) surfaces of two film converters by the fluxes of laser and X-ray radiations falling onto them. These fluxes were determined at the first stage of the calculations which numerically simulated the dynamics of fields in lateral sections (illuminators) of a composite X-ray target. In the calculations, the back action was neglected, i.e., the action of energy fluxes from the side of the central section to lateral sections of the combined holhraum.

Analysis of physical conditions in the lateral sections-illuminators showed that up to a half-duration of the laser pulse the integrity of separating partitions between the sections is broken and the laser radiation penetrates the inner space of the diagnostic section. This leads both to the additional heating of section walls and to uncontrolled action on the sample itself.

Calculations of the energy balance show that if the influence of laser radiation is neglected, then the energy of X-ray radiation from the walls of the central section is only 140 J. In this case, the energy of the laser radiation passed to the section is up to 200 J. In the frameworks of the sector approximation applied, features of propagation of laser radiation scattered in the central section cannot be found with a sufficient accuracy, which makes it impossible to take into account the action introduced by the laser radiation.

Thus, in the case of the axial injection of laser beams, a breakdown of the film partitions separating the sections of the holhraum makes it impossible to numerically predict the state of the sample under investigation. This is why we omit the calculation data concerning the conditions in the central section of the combined holhraum. We may only note that the effective temperature of X-ray radiation in the diagnostic section may reach 70–80 eV (see Fig. 6).

## 3. Lateral injection of laser radiation

The scheme of the experiments with the lateral injection of laser radiation into the internal volume of the combined holhraum is presented in Fig. 7. The changed method of injecting four laser beams substantially changes the structure of the absorbed laser energy distribution on the internal surface of lateral sections-illuminators. In this case, the absorption of laser radiation in the primary spots is higher and no zones of intense secondary irradiation arise on the surface of film converters. As a result, the partitions between holhraum sections remain intact and the laser radiation does not pass to the internal volume of the diagnostic section.

### 3.1. External section (illuminator)

Figure 8 shows the distribution of the laser radiation energy absorbed on the internal surface of a lateral section-illuminator, obtained in the model calculation with the absorption coefficient $k$ (1). One can see that laser radiation is most substantially absorbed in the zones of primary laser spots. In contrast to the axial injection of laser radiation, the scattered radiation does not form bright zones of secondary laser irradiation. (In the case of the lateral injection of laser radiation, the scattered radiation propagates inside the illuminator along screw trajectories, which eliminates concentration of laser energy in near-axis regions.)

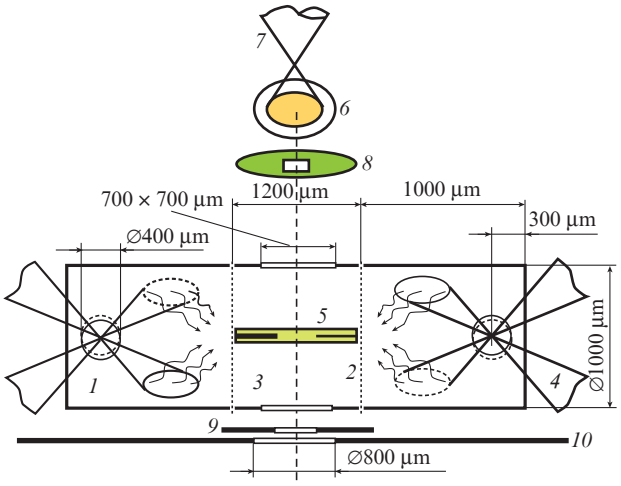


**Figure 7.** Schematic representation of experiments on investigating X-ray opacity with the injection of laser beams through two holes on the cylindrical surface of the illuminator:
(*1*) target-illuminator; (*2*) partition; (*3*) diagnostic section; (*4*) laser radiation beam; (*5*) heated material under study;(*6*) additional target; (*7*) laser radiation beam of a backlighting X-ray source; (*8*) aperture with a point hole; (*9*, *10*) protection masks.

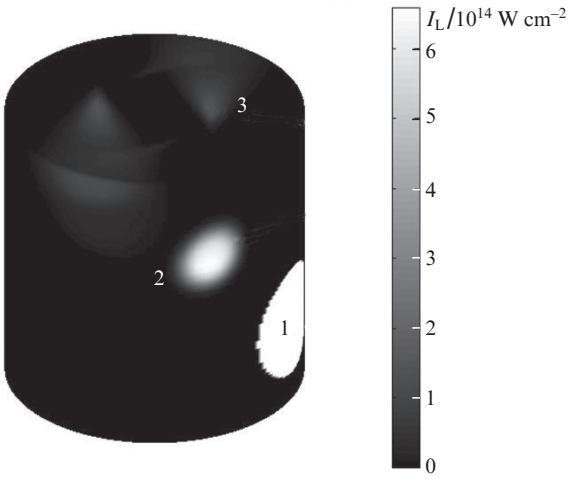


**Figure 8.** Distribution of laser radiation energy absorbed on the internal surface of the side section (lateral injection of laser beams), obtained by the model calculation with the absorption coefficient of type (1):
(1) hole for injection of laser radiation; (2, 3) primary and secondary laser spots, respectively.

The changed method for injecting laser beams results in changes in the angles of laser radiation incidence onto the internal surface of the illuminator. Figure 9 presents the time dependences of the absorption coefficient $k$ of laser radiation for various domains on the internal surface of the illuminator. One can see that more than 50% of the incident flux of the

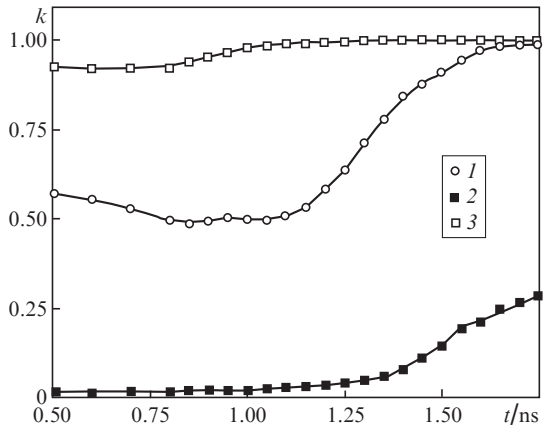


**Figure 9.** Time dependences of the absorption coefficient of laser radiation $k$ (lateral injection of laser beams) in (*1*) primary and (*2*) secondary laser spots on the film converter and (*3*) on the lateral surface of a cylindrical illuminator.

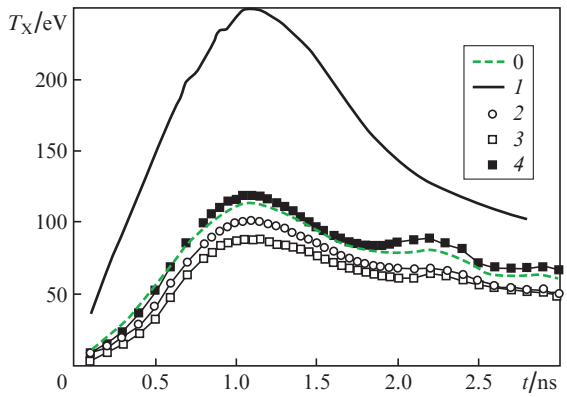


**Figure 10.** Time dependences of the effective radiation temperature on the internal surface of the illuminator in the domain of (*1*) primary laser spots, (*2*) on the film converter, (*3*) on the rear edge of illuminator and (*4*) on the lateral surface of the illuminator. The curve designated by 0 is the temperature of the X-ray radiation escaping through the holes.

laser energy is absorbed in the primary spots (compare Fig. 4), whereas for the film converter we have $k \approx 0.02$. Such a difference is explained by the fact that now the laser radiation falls onto the surface at angles of 25°–40° whereas to the surface of the film–converter it falls at angles of 60°–70°.

In sector partitioning the following areas were selected: primary laser spots – sectors 1 and 2, the film converter – sector 3, the edge of the illuminator – sector 4 and the cylindrical surface of the illuminator – sector 5. Table 2 presents the balance of the laser energy absorbed on the internal surface of the illuminator. One can see that a considerable part of laser radiation is absorbed in the zones of primary laser spots. A comparable part of laser energy is absorbed on the lateral (cylindrical) surface of the illuminator.

**Table 2.** Balance of laser energy in the illuminator in the case of the lateral injection of laser beams.

| Sector number | Sector | $S$/mm$^2$ | $E_L$/J |
|---|---|---|---|
| 0 | Holes | 0.257 | 0.15 |
| 1 | Primary laser spots | 0.029 | 136 |
| 2 | on the cylindrical surface of the illuminator | 0.029 | 136 |
| 3 | Film converter | 0.785 | 4.5 |
| 4 | Edge of the illuminator | 0.785 | 0.007 |
| 5 | Cylindrical surface of the illuminator | 2.826 | 201 |
| | $\Sigma$ | 4.712 | 478 |

Time dependences of the effective temperature of irradiation of various areas on the internal surface of illuminator are shown in Fig. 10. In the narrow zones of primary laser spots where the material is strongly heated by intense laser radiation, the radiation temperature $T_X$ reaches ~250 eV. In this case, the irradiation of these areas is much higher than that of the rest part of the internal illuminator surface. On the lateral surface the temperature of irradiation is ~120 eV, and on the surface of the separating film it is ~100 eV.

Figure 11 shows the spectra of X-ray radiation for various areas on the internal surface of the illuminator. One can see that the spectrum corresponding to primary spots comprises

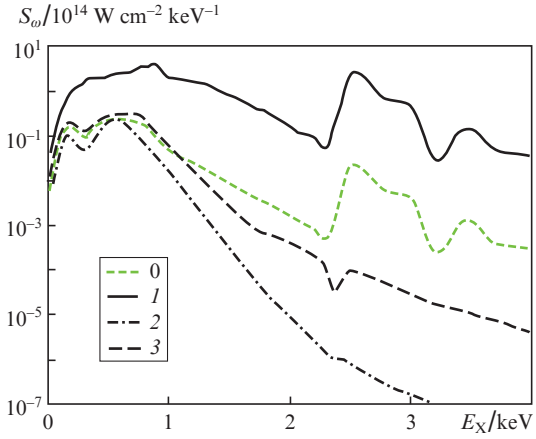


**Figure 11.** Spectra $S_\omega$ of X-ray radiation of illuminator walls (the laser beams are injected through the holes on the lateral surface of the illuminator) at the instant of maximal irradiation ($t$ = 1.15 ns) from the domain of (*1*) primary laser spots, (*2*) film converter and (*3*) lateral surface of the illuminator. The curve designated by 0 corresponds to the spectrum of radiation escaping through the holes.

a noticeable part of hard X-ray radiation of the M-band of gold with the X-ray quantum energy of 2.5–3 keV.

### 3.2. Central section

The spectral fluxes of X-ray radiation falling to an external boundary of the film–converter estimated at the first stage of calculations were used for the second-stage calculations of the conditions in the central sector of the combined holhraum by the SND-LIRA code. In the diagnostic section, sectors 1 and 2 corresponded to surfaces of the film converter, and sector 3 corresponded to the lateral surface. An additional sector 4 was separated for analysing the conditions on the surface of the sample under investigation.

Time dependences of the efficient irradiation temperature for the walls of the diagnostic sector are shown in Fig. 12. The radiation from the illuminator walls passes through the material of the film converter and heats the lateral (cylindrical) surface of the central section. The radiation temperature of the film–converter $T_X$ reaches 90 eV. A maximal radiation

temperature of the lateral surface is ~60 eV. Totally these actions produce the field of heating radiation on the sample under investigation with a temperature reaching a maximal value of ~70 eV. Spectra of radiation from the film converter and from the lateral surface of the diagnostic section are shown in Fig. 13 at the instant of maximal irradiation. Also, the spectrum of radiation falling to the sample is presented in the figure.

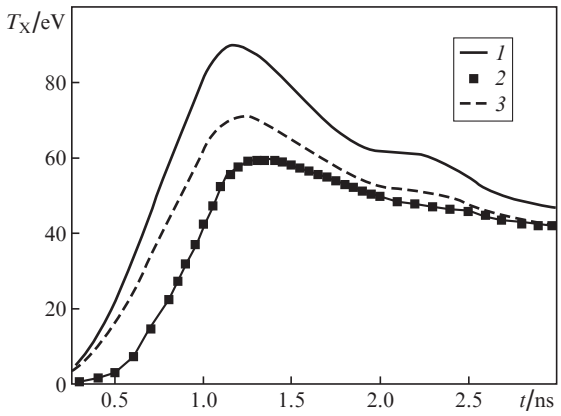


**Figure 12.** Time dependence of the effective radiation temperature of (*1*) the film converter and (*2*) the lateral surface of the central section. Curve (*3*) is the temperature of X-ray radiation falling onto the sample under study.

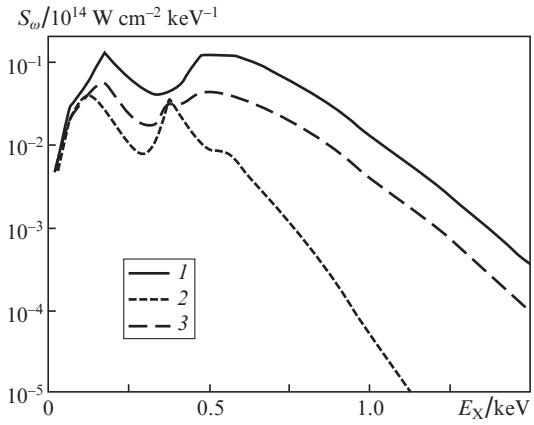


**Figure 13.** Spectra of X-ray radiation from the film converter (*1*), from lateral cylindrical surface of central section (*2*), and of radiation falling onto the sample under study (*3*).

Consider the dynamics of characteristics of the material of the sample comprised of an aluminium layer of thickness 0.2 μm placed between plastic plates of thickness 1 μm under the action of a field of heating radiation generated in the diagnostic section of the holhraum. We will assume that the irradiated sample is placed at a centre of the section for its two-side heating by quasi-thermal radiation. Distributions of density and electron temperature in the body of the sample under investigation at various instants are shown in Fig. 14. One can see that all the material of the aluminium layer is kept in the same conditions (thus, at $t$ = 1.3 ns a temperature variation over the whole layer volume does not exceed ~1 eV, and the density variation is within 4%).

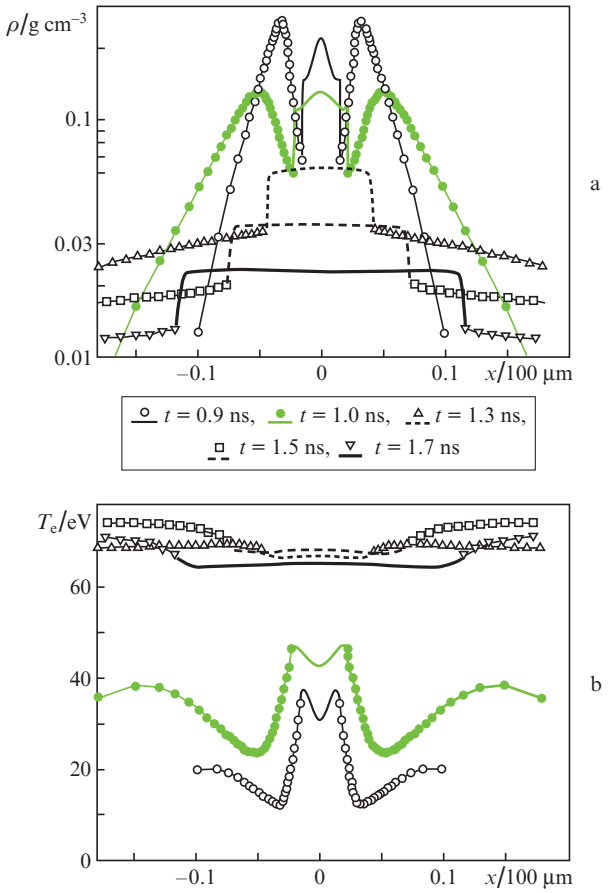


**Figure 14.** Conditions of the material of the aluminium sample (curves without marks) and of plastic covering (marked curves) under two-side heating at various instants: (a) sample density and (b) electron temperature.

## 4. Conclusions

The scheme suggested for numerical calculations of the dynamics of radiation fields (both laser and X-ray) in a three-section holhraum was applied for numerical simulation of opacity in the experiments performed at the ISKRA-5 laser facility. The scheme is based on step-by-step calculations by the numerical SND-LIRA code. At the first stage, characteristics of the X-ray radiation in lateral sections-illuminators of the holhraum are calculated, which is generated as a high-intensity laser radiation is absorbed. Also, energy fluxes are determined for laser and X-ray radiation falling onto the surface of the partition between sections, i.e., the separating film–converter. At the second stage the boundary fluxes found are employed for calculating characteristics of X-ray radiation in the central (diagnostic) section of the holhraum.

It was shown that in the case of the axial injection of four laser beams with the energy of ~900 J, intense spots of secondary laser irradiation are formed on the surface of the film converter. This leads to the burn-through of the film–converter material and passing of the laser radiation with the energy of ~200 J to the internal volume of the diagnostic section. This may result in intense additional uncontrolled action both on the walls of the central section and on the sample itself.

Also we considered a variant of the lateral injection of laser beams. It was established that no noticeably intense

zones of secondary laser irradiation are formed in this case, and localisation of laser radiation within the limits of lateral sections (illuminators) is guaranteed. In this scheme of laser beam injection, the suggested two-stage calculation scheme is successful, and the entire calculation of the dynamics of radiation fields (laser and X-ray) in a three-section holhraum can be performed in the frameworks of sector approximation. It was shown that in the case of two-side regime of heating of the sample (which is placed in the centre of the diagnostic section), highly uniform distributions of density and temperature may be provided over the volume of the material under study. The optimal delay of the backlighting X-ray pulse corresponding to uniform density and temperature distributions over the sample is 1.3–1.7 ns.

## References

1. Bondarenko S.V., Garanin R.V., Zhidkov N.V., Pinegin A.V., Suslov N.A. *Kvantovaya Elektron*., **42**, 51 (2012) [*Quantum Electron*., **42**, 51 (2012)].
2. Bel'kov S.S., Sharov O.O. *Kvantovaya Elektron*., **41**, 901 (2011) [*Quantum Electron*., **41**, 901 (2011)].
3. Bondarenko S.V., Dolgoleva G.V., Novikova E.A. *Vopr. Atom. Nauki Tekh., Ser. Mat. Model. Fiz. Prots.*, (3-4), 15 (2007).
4. Bondarenko S.V., Dolgoleva G.V., Novikova E.A. *Kvantovaya Elektron*., **37**, 372 (2007) [*Quantum Electron*., **37**, 372 (2007)].
5. Ginzburg V.L. *The Propagation of Electromagnetic Waves in Plasmas* (London: Pergamon, 1964; Moscow: Fizmatlit, 1960).